HHS Public Access

Author manuscript

Cell Rep. Author manuscript; available in PMC 2021 June 05.

Published in final edited form as:

Cell Rep. 2021 January 05; 34(1): 108588. doi:10.1016/j.celrep.2020.108588.

Small Molecule SARM1 Inhibitors Recapitulate the SARM1$^{-/-}$ Phenotype and Allow Recovery of a Metastable Pool of Axons Fated to Degenerate

Robert O. Hughes[1], **Todd Bosanac**[1], **Xianrong Mao**[2], **Thomas M. Engber**[1], **Aaron DiAntonio**[3,4], **Jeffrey Milbrandt**[2,4], **Rajesh Devraj**[1], **Raul Krauss**[1,5,*]

[1]Disarm Therapeutics, a wholly owned subsidiary of Eli Lilly & Co, Cambridge, MA 02142, USA

[2]Department of Genetics, Washington University School of Medicine, St. Louis, MO 63110, USA

[3]Department of Developmental Biology, Washington University School of Medicine, St. Louis, MO 63110, USA

[4]Hope Center for Neurological Disorders, Washington University School of Medicine, St. Louis, MO 63110, USA

[5]Lead Contact

SUMMARY

Axonal degeneration is responsible for disease progression and accumulation of disability in many neurodegenerative conditions. The axonal degenerative process can generate a metastable pool of damaged axons that remain structurally and functionally viable but fated to degenerate in the absence of external intervention. SARM1, an NADase that depletes axonal energy stores upon activation, is the central driver of an evolutionarily conserved program of axonal degeneration. We identify a potent and selective small molecule isoquinoline inhibitor of SARM1 NADase that recapitulates the SARM1$^{-/-}$ phenotype and protects axons from degeneration induced by axotomy or mitochondrial dysfunction. SARM1 inhibition post-mitochondrial injury with rotenone allows recovery and rescues axons that already entered the metastable state. We conclude that SARM1 inhibition with small molecules has the potential to treat axonopathies of the central and peripheral nervous systems by preventing axonal degeneration and by allowing functional recovery of a metastable pool of damaged, but viable, axons.

*Correspondence: rkrauss@disarmtx.com.

AUTHOR CONTRIBUTIONS

R.K. and R.O.H. jointly conceived the study. R.K. supervised the project, designed experiments, interpreted and analyzed data, and wrote the manuscript. R.O.H. and T.B. designed and supervised experiments and analyzed data leading to identification and development of small molecule chemical matter. X.M., A.D., and J.M. designed the SAM-TIR NADase assay, R.O.H., T.M.E., T.B., R.D., A.D., and J.M. edited the manuscript and contributed to interpretation of the data.

DECLARATION OF INTERESTS

R.O.H., T.B., T.M.E., R.D., and R.K. are employees and shareholders of Disarm Therapeutics, a wholly owned subsidiary of Eli Lilly & Co. R.O.H., T.B., T.M.E., R.D., R.K., A.D., X.M., and J.M. are inventors on patents related to this work. A.D. and J.M. are cofounders and shareholders of Disarm Therapeutics and members of its scientific advisory board. The authors have no other competing conflicts or financial interests.

SUPPLEMENTAL INFORMATION

Supplemental Information can be found online at https://doi.org/10.1016/j.celrep.2020.108588.

In Brief

Axonal degeneration is prevalent in neurodegenerative disorders of the central and peripheral nervous systems. Hughes et al. developed potent small molecule inhibitors of SARM1, a central driver of axonal degeneration, that protect axons and allow recovery of already-injured axons that otherwise would degenerate. SARM1 inhibition may treat axonal degeneration.

Graphical Abstract

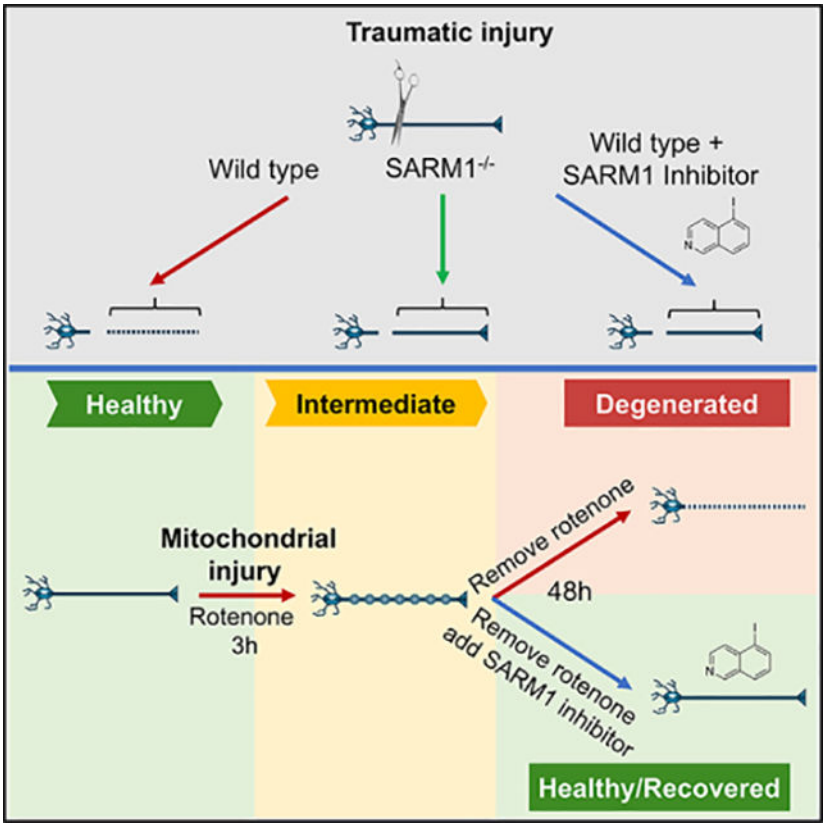

INTRODUCTION

Axonal degeneration is an early and ongoing pathophysiological event in many neurodegenerative diseases. The phenomenon of dying-back pathology, in which axonal degeneration precedes that of the cell body of the neuron (Cavanagh, 1979) is now increasingly accepted as a driver of disease progression and accumulation of disability in chronic diseases such as multiple sclerosis, Parkinson's disease, and amyotrophic lateral sclerosis (ALS) or acute conditions such as traumatic brain injury (Coleman and Höke, 2020; Figley and DiAntonio, 2020; Krauss et al., 2020). In consequence, axonal protection is an important, yet elusive, neuroprotective approach to treatment in chronic and acute CNS and peripheral nervous system (PNS) neurodegenerative disorders.

Multiple sclerosis, and its animal model, experimental acute encephalomyelitis (EAE), show substantial axonal loss either as a primary axonopathy or as a consequence of demyelination

and exposure to an inflammatory milieu (Criste et al., 2014; Wujek et al., 2002). In multiple sclerosis and EAE, axons can exist in three broad populations, which include healthy axons, transected axons that present a characteristic end bulb, and a population of axons in an intermediate state, characterized by the presence of axonal blebs and varicosities, which can accumulate β-amyloid precursor protein (β-APP) (Nikić et al., 2011). This intermediate pool of axons has also been observed in contusion models of spinal cord injury (Williams et al., 2014). Recent studies of the intermediate pool of axons have shown that they form as a result of mitochondrial dysfunction or mechanical injuries (Nikić et al., 2011; Williams et al., 2014). Importantly, these studies described that under certain circumstances, the blebs and varicosities can exist in a metastable state that can resolve, and those axons can recover a normal, healthy morphology (Nikić et al., 2011; Williams et al., 2014). The discovery of this intermediate pool of potentially recoverable axons can have important clinical implications, because in addition to protecting and preserving axons to slow or stop accumulation of disability, it may be possible to achieve a certain amount of functional improvement by shifting the equilibrium of the metastable state from prodegenerative back to recovery (Nikić et al., 2011; Williams et al., 2014).

A major molecular pathway that drives axonal degeneration was initially characterized in WldS mutant mice, which are resistant to Wallerian degeneration, as an active process that dismantles the distal axon after axotomy (reviewed in Coleman and Höke, 2020; Krauss et al., 2020). Once initiated, the axonal dismantling process proceeds through a series of steps in a manner analogous to the active processes that drive programmed cell death (Krauss et al., 2020). However, the molecular players in both processes are substantially different (Simon et al., 2012), and as a consequence, anti-apoptotic agents are ineffective at reducing axonal degeneration downstream of several insults to the axon (Simon et al., 2012). This has important therapeutic implications, because anti-apoptotic agents would not be expected to provide clinical benefit in conditions in which axonopathy is a main driver of disease pathophysiology (Athauda and Foltynie, 2015; Krauss et al., 2020).

SARM1, a unique member of the Myd88 family of adaptor proteins, has been recognized as the central mediator of axonal degeneration in pathological conditions (Gerdts et al., 2015; Osterloh et al., 2012). SARM1 loss-of-function mutants are resistant to axonal degeneration, and several *in vitro* and *in vivo* studies have demonstrated profound protection of axons in response to insults such as mechanical injuries, mitochondrial dysfunction, reactive oxygen species, and disruption of axonal transport (Loreto et al., 2020; Osterloh et al., 2012; Summers et al., 2014, 2020; Yang et al., 2015). Furthermore, studies in animal models of neurological disease have shown robust protection of axons *in vivo* (Fernandes et al., 2018; Geisler et al., 2016; Gerdts et al., 2015; Henninger et al., 2016; Marion et al., 2019; Osterloh et al., 2012; Turkiew et al., 2017; White et al., 2019; Yang et al., 2015; Ziogas and Koliatsos, 2018; Ko et al., 2020). SARM1 contains a regulated NAD^+ glycohydrolase (NADase) activity embedded within the C-terminal Toll/interleukin-1 receptor (TIR) domain of the molecule, which becomes activated upon dimerization of the TIR domains (Essuman et al., 2017). Mutations of glutamic acid residue E642, which disable catalysis, demonstrated that SARM1 enzymatic activity is required for axonal degeneration in response to injury (Essuman et al., 2017). This enzymatic activity is amenable to pharmacological inhibition and thus represents an attractive therapeutic target for neurodegenerative conditions. We

developed a biochemical assay to identify small molecule inhibitors of the SARM1 NADase and demonstrated their ability to protect axons and phenocopy SARM1 genetic loss of function through pharmacological inhibition. Furthermore, we explored the extent of axonal protection by pharmacological SARM1 inhibition post-injury and whether SARM1 inhibition could induce recovery of a metastable intermediate axonal population.

RESULTS

Identification of Isoquinoline SARM1 NADase Inhibitors

To identify small molecule inhibitors of SARM1 NADase activity, we developed a biochemical cell-lysate assay in which a recombinant construct of the constitutively active SAM-TIR protein of human SARM1 was overexpressed (Essuman et al., 2017) in mammalian cells. Using this system, we measured both production of adenosine diphosphate ribose (ADPR), a product of the hydrolysis of NAD^+ by SARM1 (Essuman et al., 2017), and the hydrolysis of NAD^+ by rapid-fire mass spectrometry. At the time we initiated this work, there were no known inhibitors of SARM1; therefore, we conducted a high-throughput screen of a collection of small molecule compounds to identify novel starting points for optimization. One hit identified was isoquinoline, compound **1** (IC_{50} = 10 μM) (Figure 1). We determined that the incorporation of substituents at the 5 position of the isoquinoline ring significantly improved the potency. As shown in Figure 1, the biochemical potency increased from 10 μM for compound **1** to 2.6 μM for 5-hydroxyisoquinoline, compound **3**. Replacing the 5-hydroxy group with halogens further increased the potency. 5-iodoisoquinoline, compound **6**, had a biochemical potency of 75 nM. Importantly, to qualify compound **6** as a suitable analog to interrogate the role of pharmacological inhibition of SARM1 NADase, we characterized its selectivity profile. Compound **6** was selective against various NAD metabolizing and pathway enzymes (e.g., NAMPT and NMNAT) (Table S1). In addition, compound **6** was selective against a wider panel of receptors and transporters (Table S2). Thus, compound **6**, subsequently called DSRM-3716, represents a potent and selective inhibitor of SARM1.

cADPR, a Marker of SARM1 Activity, Is Decreased in Injured Neurons Treated with SARM1 Inhibitors

To assess, *in cellulo*, the extent of SARM1 inhibition by isoquinolines, we measured changes in cyclic adenosine diphosphate ribose (cADPR) levels in response to SARM1 inhibitors in axotomized mouse dorsal root ganglia (DRG) axons. cADPR is a proximal biomarker that reports on the levels of SARM1 activity in cells, even though it does not participate in axonal degeneration (Sasaki et al., 2020). Metabolite analysis 5 h post-axotomy revealed that axonal injury caused a large increase in the levels of total cADPR (Figure 2A), and a large decrease in NAD^+ (Figure 2B). Treatment with the isoquinoline DSRM-3716 produced dose-dependent inhibition of cADPR increase (IC_{50} = 2.8 μM) and substantial preservation of NAD^+ in these cultures in a manner consistent with engagement and inhibition of SARM1 enzymatic NADase activity inside the cells. Although loss of NAD^+ from cut axons was not prevented completely by SARM1 inhibition, NAD^+ loss after axotomy results from the combined action of SARM1 activation, loss of synthetic ability because of fast turnover of remaining axonal NMNAT2 (Gilley and Coleman, 2010) (Figures

S6A and S6B), and continuous use of NAD^+ to support ongoing metabolic processes in preserved axons.

Isoquinoline SARM1 NADase Inhibitors Prevent Axonal Degeneration

$SARM1^{-/-}$ robustly protects distal axons after axotomy (Osterloh et al., 2012). To test whether isoquinoline SARM1 inhibitors can protect axons from Wallerian degeneration, we implemented a quantitative axonal degeneration assay using axotomized mouse DRG neurons (Sasaki et al., 2009). Although severed wild-type (WT) axons degenerated completely after 16-h axotomy, $SARM1^{-/-}$ axons were fully protected (Figure S1). When DRG neurons were treated with isoquinoline SARM1 inhibitors, we observed axonal protection in a dose-dependent manner, until reaching complete protection (Figures 3A and 3B), in a manner that was indistinguishable from axotomized $SARM1^{-/-}$ axons (Figure 3C). To obtain an independent assessment of axonal fragmentation, we also measured release of neurofilament light chain (NfL), an axonal cytoskeletal protein released after axotomy in a SARM1-dependent manner (Sasaki et al., 2020). Treatment with SARM1 inhibitor DSRM-3716 prevented NfL release from severed axons in a dose-dependent manner (Figure 3D), with an IC_{50} (1.9 μM similar to that in the fragmentation assay (2.1 μM), and NfL released into supernatants was highly correlated with fragmentation (Figure S2). Further examination of axonal morphology and fragmentation in intact (non-injured) axons demonstrated that none of the isoquinolines tested in Figure 3B had toxic effects on axonal integrity in healthy, intact neurons (Figure S3).

Consistent with selectivity for SARM1 as the mechanism responsible for axonal protection in the cellular assay, the relative ranking potency of the isoquinolines in the biochemical assay for SARM1 inhibition (Figure 1A) was maintained in axotomized neurons (Figure 3B), e.g., DSRM-3716 > **5** > **4** > **3**. Furthermore, the potency of DSRM-3716 to inhibit cADPR increase caused by axotomy (IC_{50} = 2.8 μM) was similar to the potency required to prevent axonal degeneration (IC_{50} = 2.1 μM). Consistent with SARM1 inhibition as the mechanism of action responsible for axonal protection by isoquinolines, treating $SARM1^{-/-}$ neurons with DSRM-3716 did not provide benefit beyond the robust protection observed with SARM1 genetic loss of function (Figure S4A). To rule out a role for PARP inhibition in the mechanism of action of isoquinolines in our cell assay, we tested olaparib (AZD-2281), a potent and selective dual inhibitor of PARP1 and PARP2, and confirmed that it showed no protection of injured axons under the same assay conditions as isoquinolines (Figure S4B). Altogether, these observations support that axonal protection by DSRM-3716 results from pharmacological engagement of SARM1 in axons, where it inhibits its enzymatic activity.

Further characterization of the response to isoquinolines in cells showed that they act as reversible inhibitors of the enzyme. Removing the compound from mouse DRG cultures abolished axonal protection (Figure S5).

Axons protected by SARM1 genetic loss of function have been shown to be viable and functional when assessed by maintenance of mitochondrial membrane potential (Summers et al., 2014). To test whether isoquinoline SARM1 inhibitors can also maintain mitochondrial function after axonal injury, in addition to morphological preservation of axonal structures, we monitored maintenance of mitochondrial membrane potential using the dye

tetramethylrhodamine methyl ester (TMRM). We determined that mitochondria in severed axons became dysfunctional and showed complete loss of membrane potential, assessed by loss of TMRM fluorescence (Figure 3A), whereas axotomized axons in cultures treated with DSRM-3716 maintained viable functional mitochondria that appeared indistinguishable from untransected axons (Figure 3A).

To confirm that axonal protection by isoquinoline SARM1 inhibitors is not limited to rodent neurons and can protect injured human axons, we exposed human induced pluripotent stem cell (iPSC)-derived motor neurons to the isoquinoline SARM1 inhibitor. We determined that axonal structure in human axons was preserved after axotomy, in a manner similar to mouse DRG neurites (Figures 3E and 3F).

SARM1 Inhibition Is Protective when Initiated Several Hours after Axotomy

A reversible pharmacological SARM1 inhibitor provides a unique tool to determine whether axonal protection can occur when SARM1 inhibition is initiated after injury and enzyme activation. We treated axotomized neurites at increasing intervals after axotomy, up to 5 h, which coincides with the end of the latent phase of Wallerian degeneration when axons spontaneously begin to fragment *in vitro* (Miller et al., 2009; Gilley and Coleman, 2010). We observed that complete axonal protection 16 h after axotomy could be achieved when compounds were added up to 3 h after injury. Subsequently, some ability of SARM1 inhibitors to protect severed axons was lost, but substantial (>70%) protection could be achieved even when treatment was started 5 h post-axotomy (Figure 4).

Rotenone Can Produce an Intermediate Axonal Pool of Damaged Axons

Based on our observation that the isoquinoline inhibitor could protect severed axons after axotomy, we hypothesized that it might be possible to protect injured or stressed axons that were intact but already primed to degenerate, i.e., in an intermediate state between a healthy axon and one that is already fragmented. However, the physical disconnection of axons from their cell bodies in the axotomy assay does not allow for the study of this intermediate state. Therefore, we investigated whether an intermediate state of axonal damage could be generated *in vitro* by inducing mitochondrial damage through exposure to rotenone. Inhibitors of the mitochondrial respiratory chain, such as rotenone and carbonyl cyanide 3-chlorophenylhydrazone (CCCP), produce non-traumatic SARM1-dependent axonal degeneration and decrease levels of NMNAT2, an upstream negative regulator of SARM1 (Loreto et al., 2020; Summers et al., 2020) (Figures S6A and S6B). We confirmed that SARM1 was activated by exposure to rotenone by measuring a rapid increase in cADPR levels within 3 h of exposure to 25 μM rotenone (Figure S6C). We then tested whether pretreatment with isoquinoline SARM1 inhibitors could protect axons from mitochondrial dysfunction induced by rotenone. We observed that DRG cultures exposed to 25 μM rotenone exhibited dramatic axonal degeneration 48 h later (Figures 5A and 5B), whereas axons in SARM1$^{-/-}$ neurons were protected (Figure 5B; Figure S7A). Pretreatment of WT DRG cultures with isoquinoline SARM1 inhibitor DSRM-3716 prevented axonal degeneration to the same extent as protection observed in SARM1$^{-/-}$ neurons, assessed by fragmentation (Figures 5A and 5B), or NfL released into the culture media (Figure 5C).

In the course of these experiments, we observed that rotenone induced blebbing of the axons in a manner that was reminiscent of a poorly understood process that induces blebs and varicosities in an intermediate pool of damaged axons observed in animal models (Nikić et al., 2011; Williams et al., 2014) and multiple sclerosis pathology (Nikić et al., 2011). Although axon fragmentation was prevented, in both SARM1$^{-/-}$ neurons and in WT neurons treated with rotenone + isoquinoline SARM1 inhibitor, these blebs were present in axons throughout the cultures (Figure 5A, SARM1$^{-/-}$ and WT + DSRM-3716) as a consequence of mitochondrial dysfunction independent of SARM1.

To examine the temporal appearance of these blebs, we monitored axonal morphology after exposure to rotenone for different periods. We observed that axonal blebs formed rapidly, within approximately 15 min after rotenone exposure, and were maintained but did not increase with additional exposure time (Figure 5D; Figure S7B), during at least the next 3 h. During that time, exposed axons retained viable mitochondria that maintained membrane potential assessed by the presence of TMRM fluorescence (Figure 5C, bottom panels).

To assess whether the axonal blebs induced by rotenone are similar to axonal varicosities described in Wallerian degeneration *in vivo* (Beirowski et al., 2010) and in human pathology, we characterized them by immunocytochemistry using antibodies against markers described in axonal swellings (Beirowski et al., 2010). As shown in Figure 5E, we observed that rotenone-induced blebs accumulated cytoskeletal proteins, such as βIII-tubulin and neurofilaments (neurofilament medium chain [NfM]), as well as dephosphorylated neurofilament heavy chain (NfH) detected with monoclonal antibody SMI32, a marker of axonal damage (Trapp et al., 1998), and β-APP, a marker of axonal damage and disrupted axonal transport (Coleman, 2005). We did not detect association, either positive or negative, between the presence of axonal blebs and the localization of axonal mitochondria detected by TMRM (Figure 5E), a finding that is analogous to a previous characterization of axonal spheroids produced by traumatic injury in optic nerves (Beirowski et al., 2010).

SARM1 Inhibition Protects Axons Fated to Degenerate

To understand better the consequence of this intermediate axonal injury stage on subsequent axonal integrity and function, we removed rotenone 1 and 3 h after initial exposure, by gentle rinsing of the cultures, and then examined axon structure after 48 h. We determined that removal of rotenone at those two time points was not able to prevent subsequent axonal degeneration, even though axons were still untransected and with functional mitochondria (Figure 6A). Although removal after 1 h caused ~70% degeneration, removal at 3 h led to almost complete axonal degeneration by 48 h (Figure 6B). We also assessed axonal degeneration caused by a pulse of rotenone by measuring NfL released into the culture medium. We observed that cultures exposed to a pulse of rotenone for either 1 or 3 h released as much NfL at 48 h as continuous exposure to the mitochondrial insult (Figure 6C). This demonstrated that an intermediate axonal state generated by brief exposure to rotenone fated those axons to subsequent degeneration.

The protective effect of SARM1 NADase inhibitor added post-axotomy (Figure 5) supported the concept that SARM1 inhibition might be able to prevent the subsequent degeneration of axons in untransected neurons brought to the intermediate stage. To test this hypothesis, we

exposed cultures to rotenone for 1 and 3 h, removed rotenone by gentle rinsing, and immediately treated the cells with a maximally effective concentration of 30 μM isoquinoline SARM1 inhibitor DSRM-3716. When cultures were examined 48 h later, we observed that axons that would have otherwise completely degenerated were protected by treatment with SARM1 inhibitor post-rotenone injury (Figures 6A and 6B). In addition to preventing axonal fragmentation, treatment with SARM1 inhibitor also prevented release of NfL to the culture media (Figure 6C) and reduced axonal levels of cADPR, confirming SARM1-mediated inhibition (Figure S6C). Of note, SARM1 inhibition post-injury also protected mitochondrial viability, as demonstrated by preservation of TMRM fluorescence (Figure 6A, bottom panels). Consistent with a previous report (Summers et al., 2014), rotenone also resulted in the death of approximately 60% of neuronal cell bodies at 48 h, whereas SARM1$^{-/-}$ DRG somas were noticeably protected, resulting in neuronal cell death of ~20% (Figures S7C and S7D). We determined that this neuronal toxicity was reduced to a similar extent in WT DRG neurons treated with DSRM-3716 (Figures S7C and S7D). Altogether, these data indicate that DSRM-3716 inhibits the SARM1-dependent cell destruction pathway triggered by rotenone in sensory neurons (Summers et al., 2014).

SARM1 Inhibition Promotes Recovery of Axons in the Intermediate State

Upon closer visual examination, we observed that treatment with SARM1 inhibitor after rotenone removal not only prevented axonal fragmentation but also appeared to improve their morphology and most blebs were absent (Figure 6A). These observations led us to hypothesize that in addition to prevention of axonal injury, SARM1 inhibition post-rotenone injury might be allowing recovery of axons that had already entered a stage of intermediate damage, at which they were otherwise committed to degenerate. To test this hypothesis, we monitored individual axonal blebs over the entire 48-h period by video time-lapse microscopy, starting at the time of rotenone exposure and continuing through rotenone removal and addition of SARM1 inhibitor (Figure 7A). We determined that approximately 6 h after removal of rotenone, the blebs induced by rotenone and identified at 3 h began to transect, until they were 95% transected by 18 h (Figure 7B). By contrast, addition of SARM1 inhibitor at 3 h, after removal of rotenone, led to progressive recovery of 60% of the blebs over the next 15 h (Figures 7A and 7C; Video S1). A further 30% of the blebs remained in the axons, but those axons did not transect during that period. The remaining 10% of the blebs progressed into full axonal transection (Figure 7B). These experiments demonstrated that pharmacological SARM1 inhibition post-injury allowed recovery of axons in an intermediate, metastable state of injury that would otherwise degenerate.

DISCUSSION

Axonal degeneration is a hallmark pathophysiology in several chronic and acute neurodegenerative conditions (Coleman and Höke, 2020; Krauss et al., 2020). Loss of axons is responsible for, or substantially contributes to, disease progression, loss of function, and accumulation of disability in diseases as diverse as multiple sclerosis (Criste et al., 2014), Parkinson’s disease (Tagliaferro and Burke, 2016), and chemotherapy-induced peripheral neuropathy (Geisler et al., 2019).

The central driver of Wallerian degeneration is SARM1, a tightly regulated NADase that causes a local, cell autonomous bioenergetic crisis within axons upon activation (Essuman et al., 2017). We developed a biochemical screen to find small molecule inhibitors of the SARM1 NADase, identified and further optimized a class of isoquinolines effective in the biochemical SARM1 assay, and generated DSRM-3716, a potent small molecule inhibitor that showed double-digit nM IC_{50} against recombinant SARM1, while being highly specific against other NAD^+-processing enzymes, receptors, and transporters, and that provides robust axon protection in cellular assays. A recent report described five putative SARM1 inhibitor compounds with IC_{50} values in the range of 20–145 μM using an enzymatic biochemical assay; however, their activity in axon protection assays was not examined (Loring et al., 2020). Although NAD^+-consuming enzymes such as PARP (Cantó et al., 2015), can cause neuronal death (Alano et al., 2010), they do not participate in Wallerian or Wallerian-like degeneration (Gerdts et al., 2015; Sasaki et al., 2009) or in SARM1-dependent NAD^+ consumption (Essuman et al., 2017). We further ruled out a role for participation of PARPs in the mechanism of isoquinoline axonal protection by showing that the potent dual PARP1 and PARP2 inhibitor olaparib did not contribute to axonal protection under the same assay conditions in which compound **5** and DSRM-3716 robustly prevented axonal degeneration. Previous studies by Essuman et al. (2017) showed that the highly efficient prodegenerative activity of SARM1 resides entirely within the NADase function and could be abolished by a point mutation, E642A, in the catalytic site. This suggested that pharmacological inhibition of the NADase with small molecules might be achievable to prevent Wallerian degeneration and reproduce the axonal protective phenotype observed in SARM1 genetic loss of function. Using isoquinoline SARM1 inhibitors, we were able to demonstrate in WT neurons that this hypothesis is correct. We recently described that in neurons, SARM1 activity can be monitored through levels of cADPR (Sasaki et al., 2020). Although changes in cADPR do not affect axonal degeneration, they are a direct product of SARM1 NADase and report directly on SARM1 function as a proximal biomarker of the enzyme (Sasaki et al., 2020). Monitoring changes in cADPR levels, we established that DSRM-3716 prevented increases in axonal cADPR induced by transection, or by rotenone exposure, in a dose-dependent manner. This demonstrated that isoquinolines were capable of engaging and inhibiting SARM1 in intact neurons. Our previous structural analysis of SARM1 TIR domains showed structural similarity to CD38 (Horsefield et al., 2019), another NAD^+-consuming enzyme that produces cADPR; however, CD38 does not participate in Wallerian degeneration (Sasaki et al., 2009), and DSRM-3716 showed no inhibitory activity against this enzyme, confirming that inhibition of cADPR increase in injured axons results directly from pharmacological inhibition of SARM1. Consistent with inhibition of SARM1 activity in a cellular environment, treatment with isoquinoline inhibitors robustly protected axons injured by axotomy from Wallerian degeneration, as well as axons subjected to mitochondrial injury by rotenone from a related, but slower, Wallerian-like degeneration process. The extent of axonal protection obtained by pharmacological inhibition was indistinguishable from, and reproduced, the SARM1 genetic loss-of-function phenotype (Osterloh et al., 2012). Four additional observations support that axonal protection by isoquinolines occurs through on-target inhibition of SARM1 enzymatic activity, rather than an unknown off-target mechanism within the cells. First, the relative potency of the entire chemical series in the biochemical assay was maintained in cells;

second, the potency required to inhibit cADPR increase induced by axotomy was similar to that required to prevent axonal degeneration; third, treatment of SARM1$^{-/-}$ neurons with DSRM-3716 did not provide additional benefit beyond SARM1 genetic loss of function; and fourth, isoquinolines protected axons from two different mechanisms of axonal injury, axotomy and mitochondrial dysfunction, both of which are known to be SARM1 dependent (Osterloh et al., 2012; Summers et al., 2014). Because SARM1 is a member of the MyD88 family of adaptor proteins (O'Neill and Bowie, 2007), our findings, together with the complete protection afforded by the single point mutation E642A (Essuman et al., 2017), are not consistent with an alternative model in which a prodegenerative role could be attributed to a scaffolding function of SARM1.

Mechanistically, preventing axonal degeneration before SARM1 activation in response to injury can have important therapeutic implications in a chronic disease setting, in which axons that are healthy may eventually become compromised by pathological SARM1 activation. However, the availability of pharmacological SARM1 inhibitors allowed us to investigate two additional important translational hypotheses that cannot be studied in SARM1 constitutive knockouts and would be difficult to study by other means of SARM1 inhibition, such as RNA downregulation or protein degradation, because those would take several days to be effective.

The first question is whether axonal degeneration can be prevented once SARM1 activation has occurred and axons that are still morphologically intact and functional enter a committed phase toward degeneration at a future time. Our first indication that this might be possible was obtained in the classic axotomy assay. In this model, severed axons *in vitro* enter a latent or commitment phase that lasts 4–6 h (Gilley and Coleman, 2010), after which they begin to fragment. We determined that severed axons exposed to the isoquinoline inhibitor DSRM-3716 after injury were robustly protected, even when the inhibitor was added 5 h post-axotomy, up to the end of the latent phase that precedes the initiation of Wallerian degeneration. Our results are consistent with a previous report that showed that a cytoplasmic form of NMNAT1, the protein responsible for the WldS phenotype, when transduced into distal axons after axotomy had a protective effect (Sasaki and Milbrandt, 2010). The observation that SARM1 inhibition could robustly prevent axonal degeneration after axotomy, even up to the point when the fragmentation process is set to begin, suggested to us that equivalent protection might be possible in dysfunctional axons in neurons that were still intact. To address that question, we turned to mitochondrial injury using rotenone to generate an *in vitro* system to study axons that enter an intermediate state of dysfunction, akin to what has been proposed in chronic axonopathies (Nikić et al., 2011). In this phase, axons may still appear morphologically intact and viable, possessing functional mitochondria, yet they are destined to degenerate at a future time point. These axons are characterized and identifiable by the presence of blebs or varicosities along the axolemma (Nikić et al., 2011; Williams et al., 2014). In our *in vitro* system, we demonstrated that a similar intermediate state could be generated even after a brief pulse of rotenone. Axonal blebs induced by rotenone presented numerous morphological and biochemical similarities to axonal spheroids described in human pathology (Trapp et al., 1998) and in Wallerian degeneration (Beirowski et al., 2010). Notably, they displayed accumulation of cytoskeletal proteins βIII-tubulin and neurofilaments, as well as NfH/SMI32 and β-APP, two markers of

axonal damage and disrupted axonal transport (Trapp et al., 1998; Coleman, 2005). Once initiated, this intermediate state of axonal health *in vitro* was characterized by quick SARM1 activation, revealed by increases in cADPR, and was subsequently maintained for several hours. Nevertheless, this transitional state fated axons to further and complete degeneration many hours after removal of rotenone from the cultures, even though this took place when those axons showed no signs of transections and contained viable mitochondria. Treatment with a SARM1 inhibitor, after removal of rotenone, dramatically changed their fate and provided almost complete protection from fragmentation, abolished NfL release into the culture medium, and maintained mitochondrial viability. This demonstrated that still-intact neurons that entered an intermediate phase of axonal dysfunction, caused by persistent SARM1 activation, can be prevented from progressing to inevitable axonal degeneration and neuronal cell death by inhibiting SARM1 enzymatic activity with a pharmacological agent.

The second question that was possible to address using small molecule SARM1 inhibitors relates to the prospect of reversibility and recovery of damaged axons that have already entered the intermediate phase. Recovering a dysfunctional axon goes beyond the ability to prevent its subsequent degeneration. Previous studies have demonstrated the existence of a metastable, reversible pool of damaged axons generated *in vivo* in models of inflammatory demyelination (Nikić et al., 2011; Sorbara et al., 2014) and traumatic brain injury (Williams et al., 2014). In these axons, axonal blebs attributed to mitochondrial dysfunction would persist for certain periods and subsequently would either lead to axonal transection or resolve back to a normal-appearing axon under certain circumstances (Nikić et al., 2011; Williams et al., 2014). The intermediate damaged axons generated by mitochondrial dysfunction in our cultures represented a unique opportunity to study whether SARM1 inhibition could drive recovery, assessed by resolution of axonal blebs. Indeed, although the absence of SARM1 inhibition led to 100% focal transection of blebs, exposure of intermediate damaged axons to isoquinoline SARM1 inhibitor led to progressive recovery and resolution of 60% of axonal blebs over the next 15 h and prevented transection (but not recovery) of a further 30%. At present, there is insufficient understanding of the nature of these axonal blebs, why they form, and what allows them to resolve. It appears likely that inhibition of SARM1, a strong prodegenerative signal, may allow endogenous repair mechanisms to become operant and resolve the blebs back to normal axonal morphology before they become focal points of axonal transection.

Implications for Human Disease

We have demonstrated that small molecule inhibitors of the SARM1 NADase can be developed and that pharmacological inhibition of SARM1 can recapitulate the SARM1$^{-/-}$ phenotype and be used to protect compromised axons before irreversible degeneration caused by a non-traumatic form of axonal damage. This is an important step toward building the case that a SARM1 inhibitor has therapeutic potential to treat chronic progressive neurological disorders driven by axonopathy. It is conceivable that in progressive diseases, loss of healthy axons is driven by pathological pressure, which leads to a recurrent series of stochastic events that trigger SARM1 activation. Having a pharmacological SARM1 inhibitor onboard in those chronic conditions may allow prevention of axonal loss, which would be expected to translate clinically into slowing or preventing disability progression.

The existence of an intermediate pool of axons that appear damaged, but not yet transected, and that could be protected and even recovered to health has been suspected in neurodegenerative and traumatic conditions (Nikić et al., 2011; Sorbara et al., 2014; Williams et al., 2014). Evidence for axons presenting abnormal morphology with varicosities has emerged for conditions such as multiple sclerosis and amyotrophic lateral sclerosis, among others. For example, in multiple sclerosis, and in demyelinating animal models such as cuprizone, prolonged demyelination leads first to varicosed axons and subsequently to axonal transections, but varicosities can resolve after remyelination (Xie et al., 2010). This suggests that axons that can be maintained viable for a longer period may have a better prospect at being remyelinated and restored to health. Therefore, it is conceivable that in addition to preserving function and preventing subsequent accumulation of disability by protecting axons, a certain amount of functional recovery may also take place. A better understanding of axonal blebs induced by mitochondrial dysfunction *in vitro* will be needed to determine whether they represent the same entities as pathological axonal spheroids *in vivo*, and it will be important to assess whether SARM1 inhibition leads to recovery of axonal varicosities *in vivo* in models of disease. The possibility that axons could be protected and that, in addition, an intermediate pool of damaged axons could even be recovered to health through SARM1 inhibition can have profound therapeutic implications in human disease.

STAR★METHODS

RESOURCE AVAILABILITY

Lead Contact—Further information and requests for resources and reagents should be directed to and will be fulfilled by the Lead Contact, Raul Krauss (rkrauss@disarmtx.com).

Materials Availability—Some materials may be available from the Lead Contact with a completed Materials Transfer Agreement. Restrictions may apply on some of the reagents due to limited availability and prioritization for internal use.

Data and Code Availability—The datasets supporting the current study will be made available on reasonable request

EXPERIMENTAL MODEL AND SUBJECT DETAILS

NRK1-HEK293 for protein expression—NRK1-HEK293 cells (Essuman et al., 2017), to express $SARM1_{409–700}$, were maintained in high glucose DMEM, 10% fetal bovine serum, supplemented with penicillin/streptomycin, and passaged by suspending in 0.05% trypsin.

Primary DRG cultures—For mouse dorsal root ganglia (DRG) cultures, C57BL/6J RRID:IMSR_JAX:000664, and SARM1 knockout mice, strain B6.129X1-Sarm1 < tm1Aidi > /J, RRID:IMSR_JAX:018069 were obtained from Jackson labs, Bar Harbor, ME. All animal experiments were carried out in accordance with the regulations of the German animal welfare act and the directive 2010/63/EU of the European Parliament on the protection of animals used for scientific purposes. Protocols were approved by the local

ethics committee of the Authority for Health and Consumer Protection of the city and state Hamburg ("*Behörde für Gesundheit und Verbraucherschutz"* BGV, Hamburg). Mice were housed on a 12 hr light/dark cycle with *ad libitum* access to food and water. DRGs were dissected from embryonic day 13.5 mouse embryos (~50 ganglia per embryo) and incubated with 0.05% Trypsin solution containing 0.02% EDTA at 37°C for 30 min. After 2 min gentle centrifugation trypsin solution was removed and replaced for Neurobasal medium, 10% Fetal bovine serum. Then, DRGs were triturated by gentle pipetting, cell suspensions were washed 3 times with DRG growth medium (Neurobasal medium; ThermoFisher) containing 2% B27 (ThermoFisher), 50 ng/ml 2.5S NGF (Sigma), 10 μM uridine (Sigma), 10 μM 5-fluoro-2′- deoxyuridine (Sigma), 50 U/ml penicillin, and streptomycin. After the last wash, cells were resuspended in DRG growth medium at a ratio of ~100 μL medium/50 DRGs and counted. The cell density of these suspensions was adjusted to 1×10^7 cells/ml. Cell suspensions (0.5 μl/well; 5,000 cell/well) were placed in the center of the well using 96-well tissue culture plates coated with poly-D-Lysine (0.1 mg/ml; Sigma) and laminin (3 μg/ml; ThermoFisher). Cells were allowed to adhere in a humidified tissue culture incubator (37°C, 5% CO2) for 10 min and then DRG growth medium was gently added (200 μl/96 well).

Human iPSC-derived motor neurons—Human iPSC-derived motorneurons (C1048) were obtained from Cellular Dynamics. Cells were thawed at in a 37°C water bath for 2 minutes and 30 s and transferred to Complete Maintenance Medium (iCell Neural Base Medium1, 2% iCell Neural Supplement A, 1% iCell Nervous System Supplement) + 5 μM DAPT, as described by the manufacturer, and cell density was adjusted to 10,000 cell/μl. Cell suspensions (1 μl/well; 10,000 cell/well) were placed in the center of the well using 96-well tissue culture plates coated with poly-D-Lysine (0.1 mg/ml; Sigma) and laminin (3 μg/ml; ThermoFisher). Cells were allowed to adhere in a humidified tissue culture incubator (37°C, 5% CO2) for 10 min and then Complete Maintenance Medium + 5 μM DAPT was gently added (200 μl/96 well). Cells were maintained in a humidified incubator at 37°C, 5% CO2 for two weeks with 75% of the media replaced three times/week during the first week with Complete Maintenance Medium + 5 μM DAPT and 50% of the media replaced 3 times/ week with Complete Maintenance Medium during the second week.

METHOD DETAILS

Preparation of SAM-TIR Lysate—NRK1-HEK293T cells (Essuman et al., 2017) were seeded onto 150 cm^2 flasks at 10×10^6 cells per plate. The next day, the cells were transfected with 15 μg of human SAM-TIR expression plasmid using X-TremeGENE 9 DNA Transfection Reagent. Human SAM-TIR expression plasmid consisted of a Strep-TEV-human SARM1, aminoacids 408–700, cloned in pSF-CMV-Amp using NcoI and XbaI sites. The cultures were supplemented with 1 mM nicotinamide riboside (NR) at time of transfection to minimize toxicity from SAM-TIR overexpression (Essuman et al., 2017). Forty-eight hours after transfection, cells were harvested, pelleted by centrifugation at 1,000 rpm (Sorvall ST 16R centrifuge, ThermoFisher), and washed once with cold PBS (0.01 M phosphate buffered saline NaCl 0.138 M; KCl 0.0027 M; pH 7.4). The cells were resuspended in PBS with protease inhibitors (cOmpleteTM protease inhibitor cocktail) and cell lysates were prepared by sonication (Branson Sonifer 450, output = 3, 20 episodes of stroke). The lysates were centrifuged (12,000 × g for 10 min at 4°C) to remove cell debris

and the supernatants (containing SARM1 SAM-TIR protein) were stored at −80°C for later use in the *in vitro* SARM1 SAM-TIR NADase assay (see below). Protein concentration was determined by the Bicinchoninic (BCA) method and used to normalize lysate concentrations.

SAM-TIR NADase assay—The enzymatic assay was performed in a 384-well polypropylene plate in Dulbecco's PBS buffer in a final assay volume of 20 μl. SAM-TIR lysate with a final concentration of 5 μg/ml was pre-incubated with the respective compound at 1% DMSO final assay concentration over 2h at room temperature. The reaction was initiated by addition of 5 μM final assay concentration of NAD^+ as substrate. After a 2hr incubation at room temperature, the reaction was terminated with 40 μl of stop solution of 7.5% trichloroactetic acid in acetonitrile. The NAD+ and ADPR concentrations were analyzed by online SPE-MS/MS using a RapidFire 300 (Agilent Technologies, Santa Clara, CA) coupled to an API4000 triple quadrupole mass spectrometer (AB Sciex, Framingham, MA).

Screening of Compound Libraries—An approximately 200,000 membered collection of diverse small molecules, representing a wide variety of chemotypes, was screened at a single concentration for its ability to inhibit NAD+ turnover by SARM1 in the SAM-TIR NADase assay. Hits from this initial high-throughput screen were validated in concentration response curves to provide well qualified tool SARM1 inhibitors and starting points for further optimization. The isoquinolines described in this manuscript represent a chemical series chosen for optimization.

Axon degeneration assay and compound treatment—Axon degeneration assays in mouse DRG neurons (Sasaki et al., 2009) were performed at 6–7 DIV and in human iPSC-derived motor neurons at 14 DIV. Axons that received manual axotomy using a micro-surgical blade were examined 16 hours post-axotomy. Axons injured by rotenone received 25 μM rotenone in the culture media and were examined 48 hours later for axonal fragmentation. Isoquinoline compounds were initially dissolved in DMSO to make a 10 mM stock solution, concentrations for compound treatment was as indicated in the figures and final DMSO concentration in the cultures was 0.3%. Unless otherwise indicated in the figures, cultures were pretreated with isoquinolines for 2h before injury.

Immunohistochemistry—DRG cultures were fixed in 4% paraformaldehyde (Electron Microscopy Sciences) for 20 minutes followed by gentle PBS rinse and immunostaining. Briefly, cultures were blocked in blocking solution (5% normal goat serum and 0.3% Triton X-100 in PBS) for 2 hours and then incubated overnight in primary antibody at 4°C. The following primary antibodies were used: anti-βIII-tubulin (clone TUJ-1, 1:5000; R&D Systems); anti-βAPP (MAB348, 1:100; Millipore Sigma); anti-NfM (NB300–133 1:1000; Novus Biologicals); anti dephosphorylated NfH (clone SMI32 catalog #801701; 1:250; BioLegend). Samples were gently washed 3 times with PBS and incubated with Alexa Fluor 647–conjugated goat anti-mouse, or goat anti-rabbit Alexa Fluor 488 in blocking solution (1:2000; ThermoFisher) for 1 hour at room temperature and finally washed 3X in PBS. Images were captured with an Opera Phenix Scanner (PerkinElmer) using a 20X objective.

High resolution images of axonal blebs were captured with a 63X water immersion objective.

Viable mitochondria visualization—Live neuronal cultures were incubated with 50 nM TMRM (Image-iT TMRM Reagent, ThermoFisher) for 45 mins and imaged on the Opera Phenix using a 568 nm excitation laser. Total imaging time for one 96-well plate was 75 min. After TMRM imaging, cells were rinsed 3X with PBS, fixed in 1% paraformaldehyde, and immunostained for βIII-tubulin.

Neuronal viability—Live neuronal cultures were incubated with 0.25 μM Cytotox Green (catalog # 4633, Essen Bioscience, Ann Arbor, MI) and 1 μM Cytolight red (catalog # 4706, Essen Bioscience, Ann Arbor, MI) reagents for 20 min and imaged in an IncuCyte S3 (Essen Bioscience, Ann Arbor, MI) with a 20X objective. Cell counts were obtained from images in 9 fields collected for every well, in bright-field to capture all cells and fluorescence for Cytotox green to identify dead cells.

Metabolite extraction—Metabolites from axonal lysates were extracted as described previously (Sasaki et al., 2020). Mouse DRG neurons were prepared as described above, in Experimental Models and Subject Details, and seeded at 100,000 cells/well as a 10μl spotted culture in 24 well plates and placed in a humidified CO2 incubator for 15 minutes. After allowing for cells to adhere, culture media was gently added to a final well volume of 1 ml/well. At DIV6 all axons were severed using a micro-surgical blade to cut around the cluster of neuronal cell bodies, and axons, cell bodies and supernatants were collected and analyzed separately. Complete axotomy around the cell bodies cluster was confirmed by ensuring that there were no gaps in the mark left by the blade on the surface of the tissue culture plastic. At DIV6, tissue culture plates were placed on ice and culture medium replaced with ice-cold saline (0.9% NaCl in water, 500 μL per well). For collection of axonal metabolites, cell bodies were removed using a pipette. For collection of intracellular metabolites, saline was removed and replaced with 160 μL ice cold 50% MeOH in water. The axons were incubated for a minimum of 5 min on ice with the 50% MeOH solution and then the solution was transferred to tubes containing 50 μL chloroform on ice, shaken vigorously, and centrifuged at 20,000 g for 15 min at 4°C. The clear aqueous phase (140 μl) was transferred into a microfuge tube and lyophilized under vacuum. Lyophilized samples were stored at −20°C until measurement. On the day of measurement, lyophilized samples were reconstituted with 15μl of 5 mM ammonium formate (Sigma Millipore) and centrifuged at 15,000 rpm (20,000 g) for 15min at 4°C. 10 μl of clear supernatant was analyzed by using LCMS.

Metabolite measurement—Lyophilized samples were thawed on ice and suspended in 90 μL of water with 5 mM ammonium formate (Sigma Millipore). The homogenized solution was transferred in injection vials and mixed with 10 μL of internal standard (2-chloroadenosine at 2 ng/μl), of which 75 μL was used for analysis by online solid phase extraction coupled with liquid chromatography and tandem mass spectrometry (XLC-MS/MS). Supernatants from DRG neurons were stored frozen in 1.5 mL Eppendorf tubes, thawed on ice and 10 μL were transferred in an injection vial and mixed with 80 μL of water with 5 mM ammonium formate and 10 μL of internal standard (2-chloroadenosine at 2 ng/

µl). 75 µL were used for analysis by online solid phase extraction coupled with liquid chromatography and tandem mass spectrometry (XLC-MS/MS). Online solid phase extraction coupled with liquid chromatography and tandem mass spectrometry (XLC-MS/MS): samples were injected into a SPE cartridge (2 mm inside diameter, 1 cm length, packed with C18-HD stationary phase), part of a SPE platform from Spark Holland (Emmen, the Netherlands). Thereafter the SPE cartridge was directly eluted on an Atlantis T3 column (3 µm, 2.1 × 150 mm; Waters, Milford, MA, USA) with a water/methanol with 5 mM ammonium formate gradient (0% B for 0.5 min, 0 to 40%B in 6 min, 40 to 60%B in 1 min, 60 to 100%B in 1 min, 100% B for 1 min and back to initial conditions), at a flow rate of 0.15 ml⁄min to the mass spectrometer. Metabolites (NAD, ADPR and cADPR) and the internal standard 2-chloroadenosine were analyzed on a Quantiva triple quadrupole (Thermo Electron Corporation, San Jose, CA, USA). Positive electrospray was performed on a Thermo IonMax ESI probe. To increase the sensitivity and specificity of the analysis, we worked in multiple reaction monitoring and followed the MS⁄MS transitions: NAD^+ MH+, 664.1–136.1; ADPR MH+, 560.1–136.1; cADPR MH+, 542.1–136.1; 2Cl-Ade MH+, 302.1–170.1. The spray chamber settings were as follows: heated capillary, 325°C; vaporizer temperature, 40°C; spray voltage, 3500 V; sheath gas, 50 arbitrary units; auxiliary gas 10 arbitrary units. Calibration curves were produced by using synthetic NAD, ADPR, cADPR and 2-chloroadenosine (Sigma Millipore). The amounts of metabolites in the samples were determined by using inverse linear regression of standard curves. Values are expressed as ng per 100,000 cells for axons.

Selectivity and safety panel screening—The data in Table S1 were generated at BPS Bioscience (San Diego, CA). The full list of assays and associated methods can be found at the BPS Bioscience website (https://bpsbioscience.com/screening-and-profiling). A hit selectivity panel against 30 receptors and ion channels tested by radioligand binding was performed at Eurofins Panlabs Discovery Services (Fremont, CA); methods and associated information can be found at the Eurofins website (https://www.eurofinsdiscoveryservices.com).

NfL measurement—NfL in tissue culture supernatants was measured by ELISA using the NF-Light ELISA kit from Uman Diagnostics (Umea, Sweden) using the manufacturer's instructions.

Western protein analysis—Mouse DRG neurons were cultured as spotted cultures in 96 well plates. At 6 DIV cells were treated with 25 µM rotenone, 25 µM rotenone + 30 µM DSRM-3716, or 50 µM CCCP, as described in the results section and Figure S6. Upon completion of treatment, culture media was removed, cells were gently rinsed once with 100 µl PBS and subsequently lysed with 25 µl/well of lysis buffer (10 mL RIPA, Millipore Sigma Catalog number R0278; 1 tablet cOmplete Mini, EDTA Free, Protease Inhibitor cocktail; Millipore Sigma catalog number 11873580001; 1 tablet PhosSTOP; catalog #4906845001; Millipore Sigma) was added to each well. Plates were shaken for 20 min on ice in an orbital shaker and subsequently stored at −20°C until use. Lysates were centrifuged at 13200 rpm for 5 min at 4°C and 4 µl of lysate/sample were analyzed using a Jess Simple Western Analyzer (ProteinSimple, San Jose, CA) using, simultaneously, anti-NMNAT2 Antibody

sc-515206, Santa Cruz, 1:50 and anti-β-III-Tubulin, MAB1195, R&D, Systems, 1:50. Anti-NMNAT2 and anti-β-III tubulin antibodies were detected with the Jess simple anti-mouse detection module, containing a secondary rabbit anti-mouse HRP conjugated antibody, according to the manufacturer's instructions.

Video time-lapse microscopy and analysis of individual axonal blebs—DRG cultures in 96-well plates were imaged on brightfield settings every 15 minutes with a 20X objective for 48 hours in an IncuCyte S3 (Essen Bioscience, Ann Arbor, MI). Images were collected as sequential TIFF stacks. An experimenter blinded to the identity of the image stacks identified axonal blebs at 3 h after rotenone addition and tracked them individually, frame by frame, first retrogradely to before the time of rotenone addition, to confirm that they originated from healthy appearing axons as a consequence of rotenone. Subsequently, they were tracked frame by frame after the 3h mark until they either fragmented, resolved, or the 48h recording ended, and the time of each event was annotated. The time course of each recorded event was used to conduct survival analysis using Kaplan-Meier curves, and the total percentages at 48h were used to calculate overall extent of recovery or degeneration.

QUANTIFICATION AND STATISTICAL ANALYSIS

Unless otherwise stated, data are reported as means ± standard error of the mean (SEM). All measurements were obtained from distinct samples. Statistical analyses were obtained with one-way ANOVA with Holm-Sidak post hoc for comparisons between subgroups, as appropriate, $p < 0.05$ was considered statistically significant. Curve fitting and non-linear regression curves of pharmacological dose response experiments were calculated with a least-squares fit, log(inhibitor) versus response (four parameters). All graphs and statistics were drawn and calculated with GraphPad Prism software v8.4., and details of the statistical analysis are provided in the respective figure legends.

Supplementary Material

Refer to Web version on PubMed Central for supplementary material.

ACKNOWLEDGMENTS

We thank Ken Young, Markus Ketelhot, Niels Banek, and Antoine Berthemy for their expertise in cell culture and metabolite analysis and members of Disarm Therapeutics for helpful comments and advice during the preparation of this manuscript. This study was funded by Disarm Therapeutics.

REFERENCES

Alano CC, Garnier P, Ying W, Higashi Y, Kauppinen TM, and Swanson RA (2010). NAD+ depletion is necessary and sufficient for poly(ADP-ribose) polymerase-1-mediated neuronal death. J. Neurosci. 30, 2967–2978. [PubMed: 20181594]

Athauda D, and Foltynie T (2015). The ongoing pursuit of neuroprotective therapies in Parkinson disease. Nat. Rev. Neurol. 11, 25–40. [PubMed: 25447485]

Beirowski B, Nógrádi A, Babetto E, Garcia-Alias G, and Coleman MP (2010). Mechanisms of axonal spheroid formation in central nervous system Wallerian degeneration. J. Neuropathol. Exp. Neurol. 69, 455–472. [PubMed: 20418780]

Cantó C, Menzies KJ, and Auwerx J (2015). NAD(+) Metabolism and the Control of Energy Homeostasis: A Balancing Act between Mitochondria and the Nucleus. Cell Metab. 22, 31–53. [PubMed: 26118927]

Cavanagh JB (1979). The 'dying back' process. A common denominator in many naturally occurring and toxic neuropathies. Arch. Pathol. Lab. Med. 103, 659–664. [PubMed: 389195]

Coleman M (2005). Axon degeneration mechanisms: commonality amid diversity. Nat. Rev. Neurosci. 6, 889–898. [PubMed: 16224497]

Coleman MP, and Höke A (2020). Programmed axon degeneration: from mouse to mechanism to medicine. Nat. Rev. Neurosci. 21, 183–196. [PubMed: 32152523]

Criste G, Trapp B, and Dutta R (2014). Axonal loss in multiple sclerosis: causes and mechanisms. Handb. Clin. Neurol. 122, 101–113. [PubMed: 24507515]

Essuman K, Summers DW, Sasaki Y, Mao X, DiAntonio A, and Milbrandt J (2017). The SARM1 Toll/Interleukin-1 Receptor Domain Possesses Intrinsic NAD^+ Cleavage Activity that Promotes Pathological Axonal Degeneration. Neuron 93, 1334–1343.e5. [PubMed: 28334607]

Fernandes KA, Mitchell KL, Patel A, Marola OJ, Shrager P, Zack DJ, Libby RT, and Welsbie DS (2018). Role of SARM1 and DR6 in retinal ganglion cell axonal and somal degeneration following axonal injury. Exp. Eye Res. 171, 54–61. [PubMed: 29526794]

Figley MD, and DiAntonio A (2020). The SARM1 axon degeneration pathway: control of the NAD^+ metabolome regulates axon survival in health and disease. Curr. Opin. Neurobiol. 63, 59–66. [PubMed: 32311648]

Geisler S, Doan RA, Strickland A, Huang X, Milbrandt J, and DiAntonio A (2016). Prevention of vincristine-induced peripheral neuropathy by genetic deletion of SARM1 in mice. Brain 139, 3092–3108. [PubMed: 27797810]

Geisler S, Doan RA, Cheng GC, Cetinkaya-Fisgin A, Huang SX, Höke A, Milbrandt J, and DiAntonio A (2019). Vincristine and bortezomib use distinct upstream mechanisms to activate a common SARM1-dependent axon degeneration program. JCI Insight 4, e129920.

Gerdts J, Brace EJ, Sasaki Y, DiAntonio A, and Milbrandt J (2015). SARM1 activation triggers axon degeneration locally via NAD^+ destruction. Science 348, 453–457. [PubMed: 25908823]

Gilley J, and Coleman MP (2010). Endogenous Nmnat2 is an essential survival factor for maintenance of healthy axons. PLoS Biol. 8, e1000300. [PubMed: 20126265]

Henninger N, Bouley J, Sikoglu EM, An J, Moore CM, King JA, Bowser R, Freeman MR, and Brown RH Jr. (2016). Attenuated traumatic axonal injury and improved functional outcome after traumatic brain injury in mice lacking Sarm1. Brain 139, 1094–1105. [PubMed: 26912636]

Horsefield S, Burdett H, Zhang X, Manik MK, Shi Y, Chen J, Qi T, Gilley J, Lai J-S, Rank MX, et al. (2019). NAD^+ cleavage activity by animal and plant TIR domains in cell death pathways. Science 365, 793–799. [PubMed: 31439792]

Ko KW, Milbrandt J, and DiAntonio A (2020). SARM1 acts downstream of neuroinflammatory and necroptotic signaling to induce axon degeneration. J. Cell Biol. 219, e201912047. [PubMed: 32609299]

Krauss R, Bosanac T, Devraj R, Engber T, and Hughes RO (2020). Axons Matter: The Promise of Treating Neurodegenerative Disorders by Targeting SARM1-Mediated Axonal Degeneration. Trends Pharmacol. Sci. 41, 281–293. [PubMed: 32107050]

Loreto A, Hill CS, Hewitt VL, Orsomando G, Angeletti C, Gilley J, Lucci C, Sanchez-Martinez A, Whitworth AJ, Conforti L, et al. (2020). Mitochondrial impairment activates the Wallerian pathway through depletion of NMNAT2 leading to SARM1-dependent axon degeneration. Neurobiol. Dis. 134, 104678. [PubMed: 31740269]

Loring HS, Parelkar SS, Mondal S, and Thompson PR (2020). Identification of the first noncompetitive SARM1 inhibitors. Bioorg. Med. Chem. 28, 115644. [PubMed: 32828421]

Marion CM, McDaniel DP, and Armstrong RC (2019). Sarm1 deletion reduces axon damage, demyelination, and white matter atrophy after experimental traumatic brain injury. Exp. Neurol. 321, 113040. [PubMed: 31445042]

Miller BR, Press C, Daniels RW, Sasaki Y, Milbrandt J, and DiAntonio A (2009). A dual leucine kinase-dependent axon self-destruction program promotes Wallerian degeneration. Nat. Neurosci. 12, 387–389. [PubMed: 19287387]

Nikić I, Merkler D, Sorbara C, Brinkoetter M, Kreutzfeldt M, Bareyre FM, Brück W, Bishop D, Misgeld T, and Kerschensteiner M (2011). A reversible form of axon damage in experimental autoimmune encephalomyelitis and multiple sclerosis. Nat. Med. 17, 495–499. [PubMed: 21441916]

O'Neill LAJ, and Bowie AG (2007). The family of five: TIR-domain-containing adaptors in Toll-like receptor signalling. Nat. Rev. Immunol. 7, 353–364. [PubMed: 17457343]

Osterloh JM, Yang J, Rooney TM, Fox AN, Adalbert R, Powell EH, Sheehan AE, Avery MA, Hackett R, Logan MA, et al. (2012). dSarm/Sarm1 is required for activation of an injury-induced axon death pathway. Science 337, 481–484. [PubMed: 22678360]

Sasaki Y, and Milbrandt J (2010). Axonal degeneration is blocked by nicotinamide mononucleotide adenylyltransferase (Nmnat) protein transduction into transected axons. J. Biol. Chem. 285, 41211–41215. [PubMed: 21071441]

Sasaki Y, Vohra BPS, Lund FE, and Milbrandt J (2009). Nicotinamide mononucleotide adenylyl transferase-mediated axonal protection requires enzymatic activity but not increased levels of neuronal nicotinamide adenine dinucleotide. J. Neurosci. 29, 5525–5535. [PubMed: 19403820]

Sasaki Y, Engber TM, Hughes RO, Figley MD, Wu T, Bosanac T, Devraj R, Milbrandt J, Krauss R, and DiAntonio A (2020). cADPR is a gene dosage-sensitive biomarker of SARM1 activity in healthy, compromised, and degenerating axons. Exp. Neurol. 329, 113252. [PubMed: 32087251]

Simon DJ, Weimer RM, McLaughlin T, Kallop D, Stanger K, Yang J, O'Leary DDM, Hannoush RN, and Tessier-Lavigne M (2012). A caspase cascade regulating developmental axon degeneration. J. Neurosci. 32, 17540–17553. [PubMed: 23223278]

Sorbara CD, Wagner NE, Ladwig A, Nikić I, Merkler D, Kleele T, Marinković P, Naumann R, Godinho L, Bareyre FM, et al. (2014). Pervasive axonal transport deficits in multiple sclerosis models. Neuron 84, 1183–1190. [PubMed: 25433639]

Summers DW, DiAntonio A, and Milbrandt J (2014). Mitochondrial dysfunction induces Sarm1-dependent cell death in sensory neurons. J. Neurosci. 34, 9338–9350. [PubMed: 25009267]

Summers DW, Frey E, Walker LJ, Milbrandt J, and DiAntonio A (2020). DLK Activation Synergizes with Mitochondrial Dysfunction to Downregulate Axon Survival Factors and Promote SARM1-Dependent Axon Degeneration. Mol. Neurobiol. 57, 1146–1158. [PubMed: 31696428]

Tagliaferro P, and Burke RE (2016). Retrograde Axonal Degeneration in Parkinson Disease. J. Parkinsons Dis. 6, 1–15.

Trapp BD, Peterson J, Ransohoff RM, Rudick R, Mörk S, and Bö L (1998). Axonal transection in the lesions of multiple sclerosis. N. Engl. J. Med. 338, 278–285. [PubMed: 9445407]

Turkiew E, Falconer D, Reed N, and Höke A (2017). Deletion of Sarm1 gene is neuroprotective in two models of peripheral neuropathy. J. Peripher. Nerv. Syst. 22, 162–171. [PubMed: 28485482]

White MA, Lin Z, Kim E, Henstridge CM, Pena Altamira E, Hunt CK, Burchill E, Callaghan I, Loreto A, Brown-Wright H, Mead R, Simmons C, Cash D, Coleman MP, and Sreedharan J (2019). Sarm1 deletion suppresses TDP-43-linked motor neuron degeneration and cortical spine loss. Acta Neuropathol. Commun. 7, 166. 10.1186/s40478-019-0800-9. [PubMed: 31661035]

Williams PR, Marincu B-N, Sorbara CD, Mahler CF, Schumacher A-M, Griesbeck O, Kerschensteiner M, and Misgeld T (2014). A recoverable state of axon injury persists for hours after spinal cord contusion *in vivo*. Nat. Commun. 5, 5683. [PubMed: 25511170]

Wujek JR, Bjartmar C, Richer E, Ransohoff RM, Yu M, Tuohy VK, and Trapp BD (2002). Axon loss in the spinal cord determines permanent neurological disability in an animal model of multiple sclerosis. J. Neuropathol. Exp. Neurol. 61, 23–32. [PubMed: 11829341]

Xie M, Tobin JE, Budde MD, Chen C-I, Trinkaus K, Cross AH, McDaniel DP, Song S-K, and Armstrong RC (2010). Rostrocaudal analysis of corpus callosum demyelination and axon damage across disease stages refines diffusion tensor imaging correlations with pathological features. J. Neuropathol. Exp. Neurol. 69, 704–716. [PubMed: 20535036]

Yang J, Wu Z, Renier N, Simon DJ, Uryu K, Park DS, Greer PA, Tournier C, Davis RJ, and Tessier-Lavigne M (2015). Pathological axonal death through a MAPK cascade that triggers a local energy deficit. Cell 160, 161–176. [PubMed: 25594179]

Ziogas NK, and Koliatsos VE (2018). Primary Traumatic Axonopathy in Mice Subjected to Impact Acceleration: A Reappraisal of Pathology and Mechanisms with High-Resolution Anatomical Methods. J. Neurosci. 38, 4031–4047. [PubMed: 29567804]

Highlights

- Inhibitors of SARM1 NADase recapitulate SARM1$^{-/-}$ phenotype and protect injured axons
- Transient mitochondrial injury generates an intermediate state of axonal damage
- Axons entering the intermediate state of damage are fated to subsequent degeneration
- SARM1 inhibitors allow recovery of axons already in the intermediate injury state

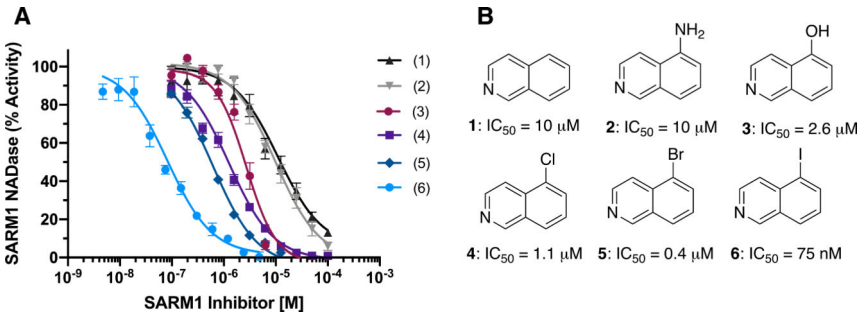

Figure 1. Identification of Isoquinoline Inhibitors of SARM1 NADase

(A) Enzymatic assay for NAD+ hydrolysis, monitored by production of the SARM1 product ADPR, using constitutively active SARM1 constructs containing the SAM-TIR domain. The curve shows inhibition of ADPR production by isoquinolines compounds **1–6**. Values represent mean ± SEM; compounds **1** n= 4, **2** n = 6, **3** n = 10, **4** n = 8, **5** n = 10, **6** n = 10.

(B) Isoquinoline series showing compound **1** identified as a weak inhibitor of ADPR production by NAD+ hydrolysis. Incorporation of substituents in position 5 of the isoquinoline ring improved potency and specificity, leading to compound **6**, subsequently referred as DSRM-3716.

See also Tables S1 and S2.

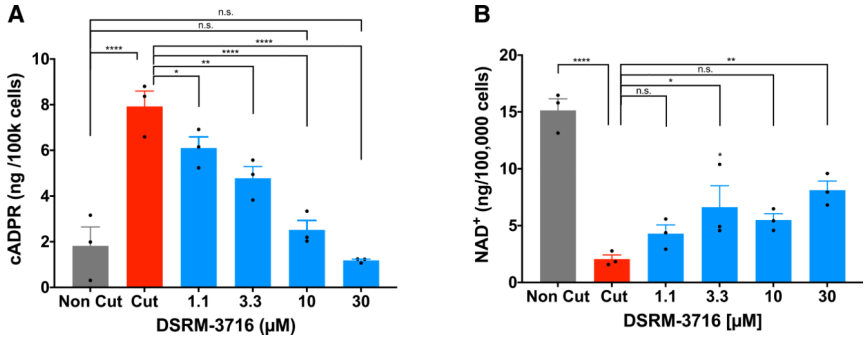

Figure 2. Isoquinolines Inhibit SARM1 Activity Caused by Axotomy

DRG neurons were treated with the isoquinoline SARM1 inhibitor DSRM-3716 at the concentrations indicated and subjected to axotomy. Metabolites from axonal lysates were prepared 4 h after axotomy and analyzed by mass spectrometry as described in STAR Methods.

(A) cADPR increase 4 h after axotomy was inhibited in a dose-dependent manner by DSRM-3716. $F(5,12) = 23.35$, $p < 0.0001$. Values represent mean ± SEM, n = 3/condition.

(B) Dose-dependent inhibition of NAD+ consumption after axotomy. $F(5,12) = 19.35$, $p < 0.0001$. Mean ± SEM, n = 3/condition.

One-way ANOVA with Holm-Sidak post hoc; *$p < 0.05$, **$p < 0.01$, ****$p < 0.0001$, n.s. = not significant; representative of 2 independent experiments with similar results.

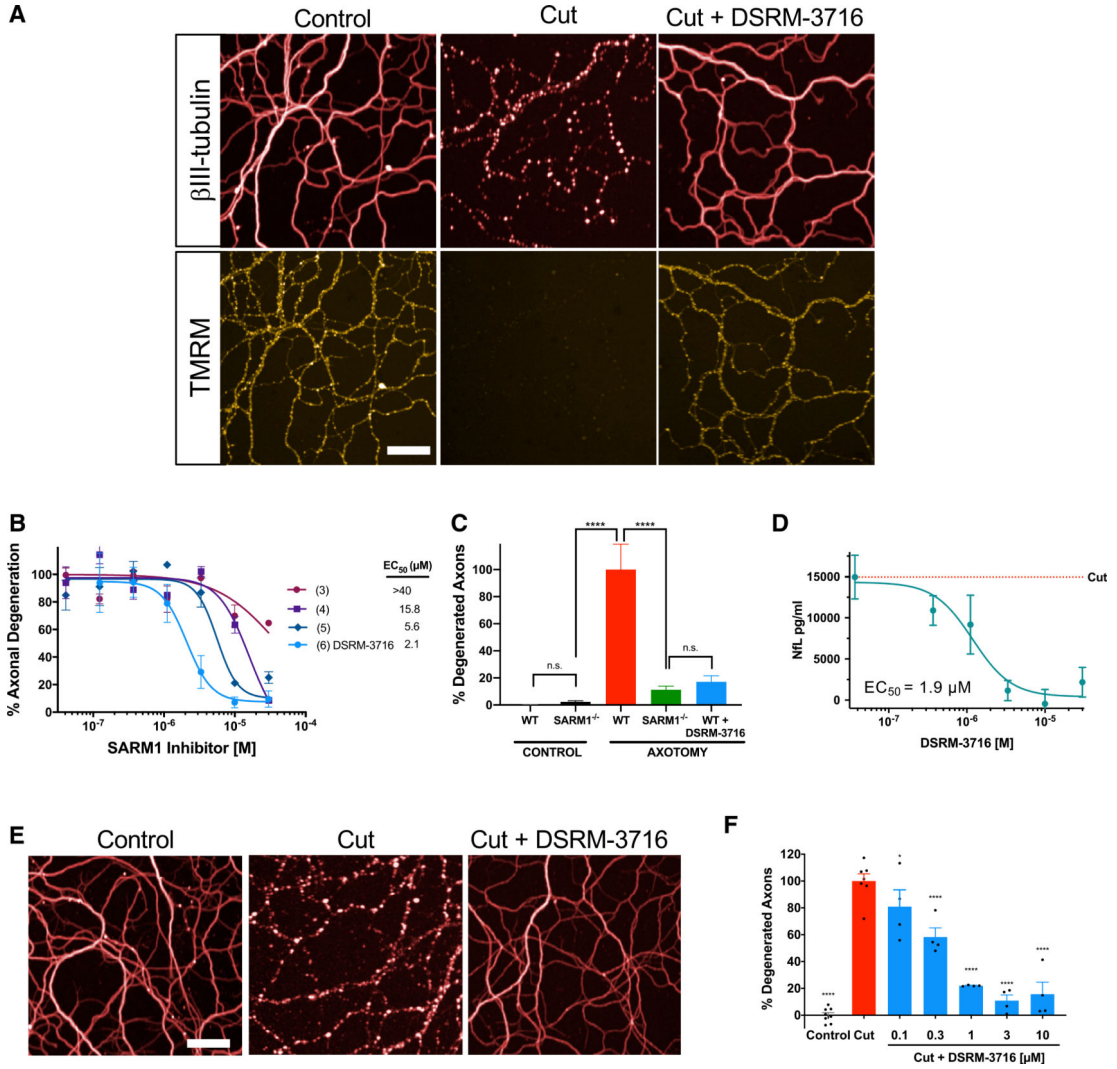

Figure 3. Isoquinoline SARM1 Inhibitor Reproduces the Axonal Protective SARM1$^{-/-}$ Phenotype

(A) 10 μM SARM1 inhibitor DSRM-3716 protected axons in mouse DRG neurons subject to axotomy (right panels). TMRM fluorescence was used to assess mitochondrial viability. Cut axons lost TMRM fluorescence, whereas axons treated with DSRM-3716 at 10 μM preserved TMRM fluorescence. Scale bar, 50 μm.

(B) Quantification of fragmentation showed that axonal protection with isoquinolines was dose dependent. Values represent mean ± SEM; compounds **3–5** n= 3, DSRM-3716 n = 7; representative of at least 10 independent experiments with similar results.

(C) Axotomized SARM1$^{-/-}$ and WT mouse DRG neurons treated with 10 μM DSRM-3716 showed similar axonal protection. One-way ANOVA with Holm-Sidak post hoc, $F(4,14) = 22.11$, $p < 0.0001$. Values represent mean ± SEM; WT + DSRM-3716 n = 3, all others n = 4; ****$p < 0.0001$, n.s. = not significant.

(D) Axonal damage was assessed by release of NfL to culture supernatants. Cultures treated with DSRM-3716 showed dose-dependent inhibition of NfL release with EC_{50} = 1.9 μM. Mean ± SEM, n = 4, representative of 5 independent experiments with similar results.

(E) Human iPSC-derived motor neurons were treated with 10 μM SARM1 inhibitor DSRM-3716 and subject to axotomy (right panel). Scale bar, 50 μm.

(F) Quantification of fragmentation in human motor neuron iPSCs showed dose-dependent protection by DSRM-3716. One-way ANOVA with Holm-Sidak post hoc, $F(6,28) = 49.07$, $p < 0.0001$. Mean ± SEM; control n = 8, cut n = 7, all doses n = 4; *$p < 0.05$, ****$p < 0.0001$; representative of 4 independent experiments with similar results.

See also Figures S1–S5.

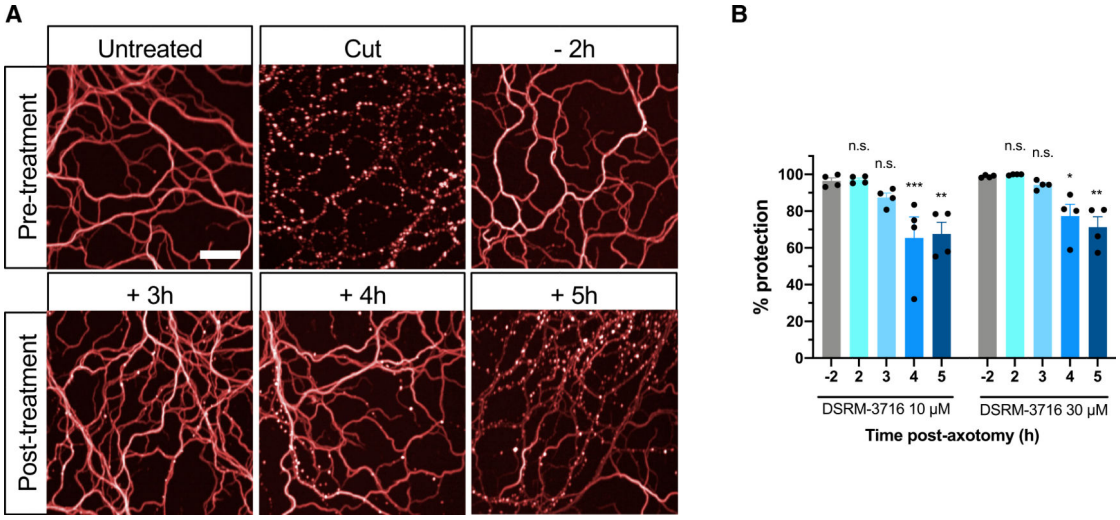

Figure 4. Pharmacological SARM1 Inhibition Protects Axons after Injury

(A) Mouse DRG neurons were subject to axotomy, and 30 μM SARM1 inhibitor was added at the times indicated in the figure. Scale bar, 50 μm.

(B) Quantification of axonal protection adding compound at the times indicated after injury at 10 and 30 μM shows that addition of SARM1 inhibitor after injury provided complete protection up to 3 h after injury and partial protection thereafter. Extent of protection was assessed at 16 h after axotomy. Two-way ANOVA with Tukey post hoc. For time of compound addition, $F(4,30) = 15.73$, $p < 0.0001$. Mean ± SEM; n = 4; *p < 0.05, **p < 0.01, ***p < 0.001, n.s. = not significant; representative of 2 independent experiments with similar results.

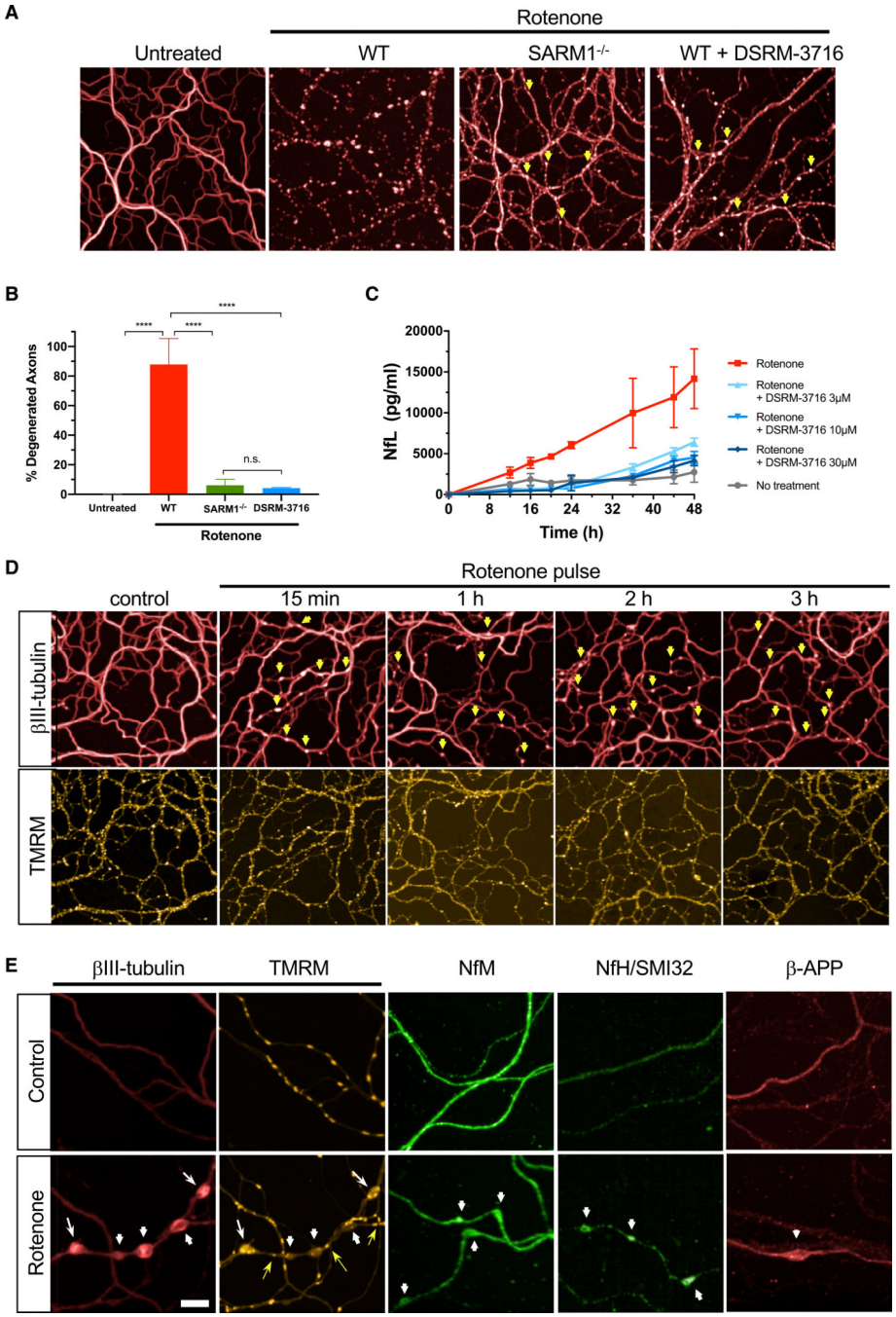

Figure 5. Pharmacological SARM1 Inhibition Protects from Rotenone-Induced Axonal Degeneration

(A) WT mouse DRGs exposed to 25 μM rotenone showed complete axonal degeneration after 48 h (second panel). Axons in SARM1$^{-/-}$ neurons (third panel) and WT neurons treated with 30 μM DSRM-3716 (right panel) did not fragment. Scale bar, 50 μm.

(B) Quantification of axonal degeneration in cells treated with 25 μM rotenone + 30 μM DSRM-3716 show robust protection comparable to protection from 25 μM rotenone observed in axons from SARM1$^{-/-}$. One-way ANOVA with Holm-Sidak post hoc, $F(3,16) = 51.45$, $p < 0.0001$. Mean ± SEM; untreated n = 8, WT n = 3, SARM1$^{-/-}$ n = 3, WT +

DSRM-3716 n = 6; ****p < 0.0001, n.s. = not significant, representative of 6 independent experiments with similar results.

(C) NfL is released over time into the culture supernatant in response to 25 μM rotenone and can be prevented by DSRM-3716. Mean ± SEM; n = 3.

(D) Mouse DRG neurons were exposed to rotenone for the times indicated and examined for axonal morphology (top panels) and TMRM fluorescence (bottom panels). Yellow arrowheads indicate axonal blebs induced by rotenone, appearing 15 min after rotenone (earliest time examined), and maintained for 3 h. TMRM fluorescence was maintained during the 3-h period. Representative images of n = 4. Scale bar, 50 μm.

(E) Close examination of axons treated with 25 μM rotenone for 3 h shows accumulation of βIII-tubulin, NfM, dephosphorylated NfH/SMI32, and β-APP in axonal blebs (arrows) compared with non-swollen areas of the same axon and to control axons. Using TMRM fluorescence, we found no specific association between mitochondria and axonal blebs. White arrowheads: blebs with few mitochondria; white arrows: blebs with several mitochondria; yellow arrows: mitochondria outside blebbed portions of compromised axons. Scale bar, 10 μm.

See also Figures S6 and S7.

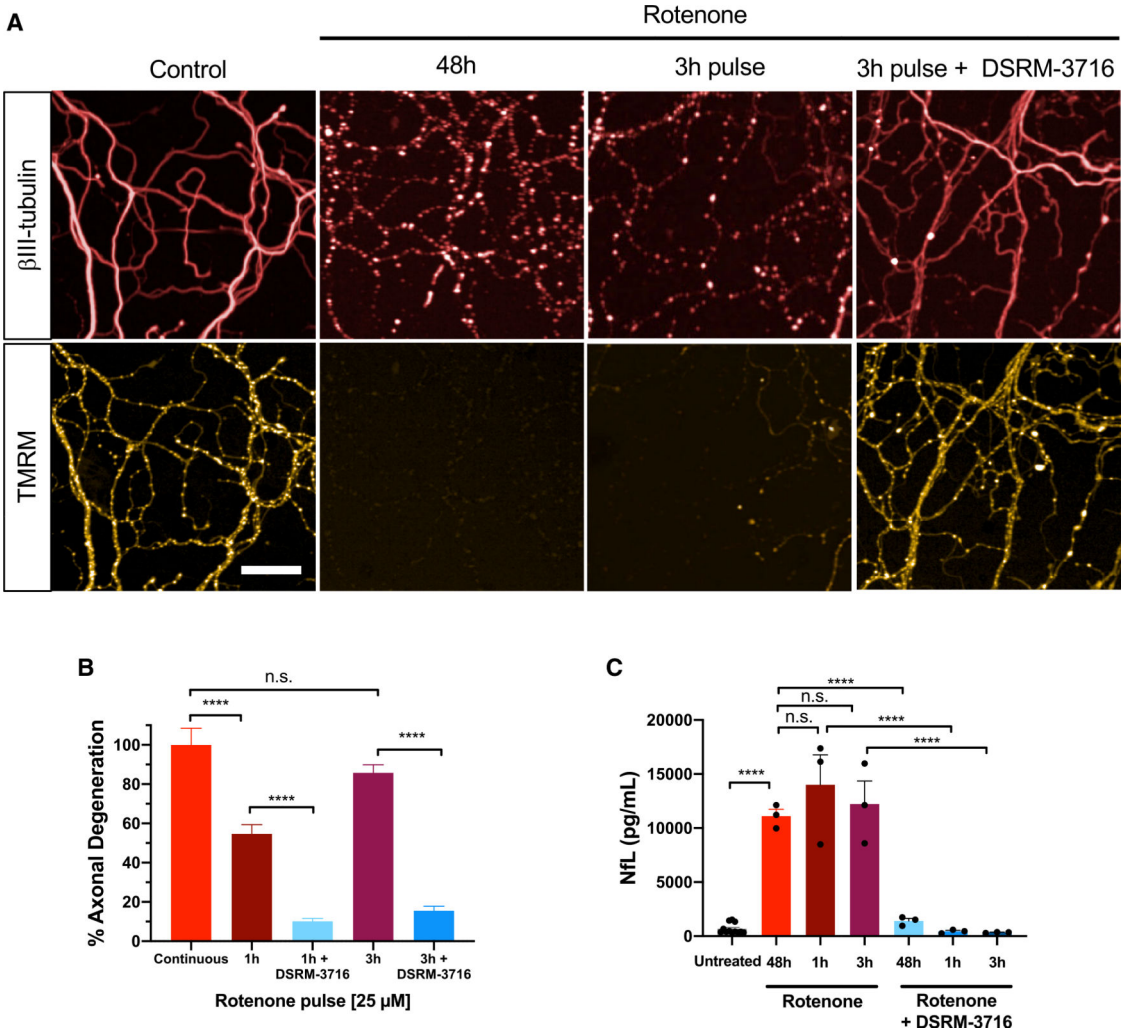

Figure 6. Pharmacological SARM1 Inhibition Protects Axons Fated to Degenerate

Mouse DRG neurons were exposed to a 3-h pulse of 25 μM rotenone and rinsed 3×. Immediately after rotenone removal, a subset of cultures received 30 μM DSRM-3716. All cells were examined 48 h after initial exposure to rotenone.

(A) Cells treated as indicated were examined for axonal morphology (top panels) and mitochondrial function by TMRM (bottom panels) as in Figure 5D. A 3-h pulse of rotenone induced complete axonal degeneration similar to continuous exposure to rotenone. In both instances, axons lost TMRM fluorescence. Treatment with 30 μM DSRM-3716 immediately after rotenone removal protected axons from fragmentation and preserved mitochondrial function assessed by TMRM fluorescence. Representative images of n = 4. Scale bar, 50 μm.

(B) Quantification of axonal fragmentation after 1- or 3-h pulses of 25 μM rotenone compared with continuous exposure in the experiment described in (A). One-way ANOVA with Sidak post hoc, $F(5,36) = 126.6$, $p < 0.0001$. Untreated n = 12, treated n = 6; representative of 5 experiments with similar results.

(C) Quantification of NfL released into the culture media also showed comparable levels of axonal damage by rotenone pulses compared with continuous exposure, which was protected by 30 μM DSRM-3716. SARM1 inhibitor was added at the time of treatment for continuous

exposure to rotenone or immediately after rotenone removal. One-way ANOVA with Sidak post hoc, $F(6,23) = 43.05$, $p < 0.0001$. Mean ± SEM; untreated n = 12, all other groups n = 3; ****$p < 0.0001$, n.s. = not significant.

See also Figures S6C and S7C.

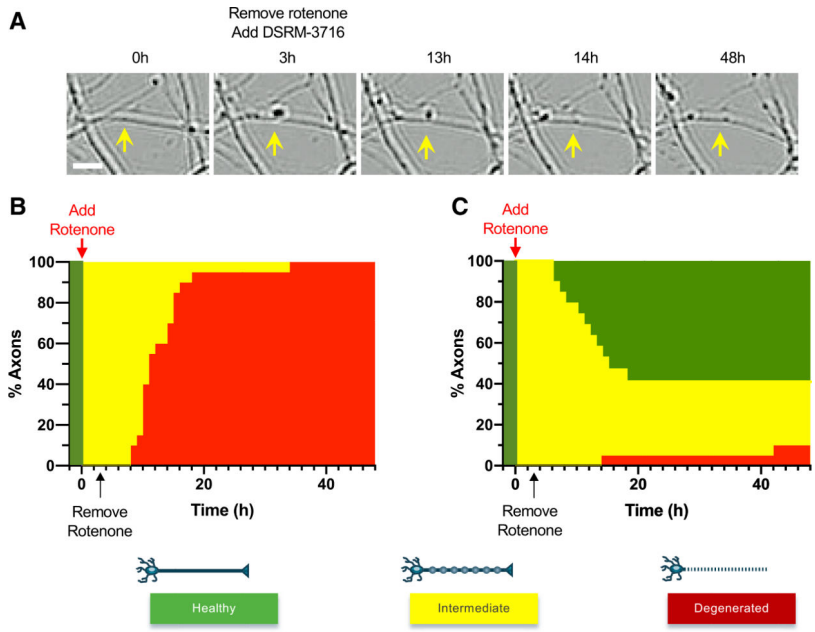

Figure 7. Pharmacological SARM1 Inhibition Allows Recovery from an Intermediate Metastable Stage of Axonal Damage

Mouse DRG neurons were exposed to a 3-h pulse of 25 μM rotenone, and immediately after rotenone removal, a subset of cultures received 30 μM SARM1 inhibitor DSRM-3716.

(A) Example of an axonal bleb formed by exposure to rotenone (yellow arrow), which recovered after treatment with 30 μM DSRM-3716. Scale bar, 10 μm.

(B) Kaplan-Meir survival curves in cultures from which rotenone was removed show that axonal blebs induced by rotenone fragmented over time until reaching 100% by 48 h.

(C) Kaplan-Meir survival curves in cultures to which 30 μM SARM1 inhibitor was added immediately after rotenone removal show that by 48 h, 60% of axonal blebs induced by rotenone reverted over time, 30% remained, and 10% fragmented. Green, healthy axons with no blebs; yellow, intermediate stage of axonal damage consisting of axonal blebs; red, individual blebs that underwent axonal transection.

See also Videos S1 and S2.

KEY RESOURCES TABLE

REAGENT or RESOURCE	SOURCE	IDENTIFIER
Antibodies		
Mouse anti-beta-III tubulin (clone TuJ1)	R&D Systems	Cat# MAB1195; RRID:AB_357520
Mouse anti-NMNAT2	Santa Cruz Biotechnology	Cat# sc-515206: RRID:AB_2827765
Alexa Fluor 647 Goat anti-mouse IgG	ThermoFisher	Cat# A21236; RRID:AB_2535805
Mouse anti-amyloid precursor protein (beta-APP)	Millipore Sigma	Cat# MAB348; RRID:AB_94882
Rabbit anti-amyloid precursor protein, clone Y188	Abcam	Cat# ab32136; RRID:AB_2289606
Rabbit anti-neurofilament medium chain (NF-M)	Novus Biologicals	Cat# NB300-133; RRID:AB_10003524
Mouse anti-Neurofilament H (NF-H) non phosphorylated (clone SMI32)	BioLegend	Cat# 801701; RRID:AB_2564642
Chemicals, Peptides, and Recombinant Proteins		
DSRM-3716	This paper	N/A
X-tremeGENE 9 DNA	Millipore Sigma	Cat# 6365787001
cOmplete, EDTA-free Protease Inhibitor Cocktail	Millipore Sigma	Cat# 11873580001
hSARM1 aa409-700	This paper	N/A
TMRM Image-iT TMRM Reagent	ThermoFisher Scientific	Cat# I34361
iCell Motorneurons Media Kit	Cellular Dynamics	Cat# R1152
Laminin, Mouse, natural	ThermoFisher	Cat# 23017015
Nerve growth factor (NGF) 2.5 s	Millipore Sigma	Cat# N6009-4X25UG
Neurobasal Medium	ThermoFisher	Cat# 21103049
Penicillin-Streptomycin (10,000 U/mL)	ThermoFisher	Cat# 15140122
Poly-D-lysine hydrobromide	Millipore Sigma	Cat# P7280
Trypsin-EDTA (0.25%), phenol red	ThermoFisher	Cat# 25300054
Uridine	Millipore Sigma	Cat# U3003; CAS 58-96-8
5-Fluoro-2′-deoxyuridine (FUDR)	Millipore Sigma	Cat# F0503; CAS 50-91-9
B-27 Supplement, serum free	ThermoFisher	Cat# 17504044
D-(+)-Glucose solution	Millipore Sigma	Cat# G8644; CAS 50-99-7
Paraformaldehyde, 32% solution	Electron Microscopy Sciences	Cat# 15714-S; CAS 50-00-0
Anti-Mouse detection module	Protein Simple	DM-002
DAPT	Millipore Sigma	Cat# D5942; CAS 208255-80-5
iCell Neural Base Medium 1	Cellular Dynamics	Cat# M1010
iCell Neural Supplement A	Cellular Dynamics	Cat# M1032
iCell Nervous System Supplement	Cellular Dynamics	Cat# M1031
2-Chloro adenosine	Millipore Sigma	Cat# C-5134; CAS 146-77-0
Cyclic adenosine diphosphate ribose (cADPR)	Millipore Sigma	Cat# C-7344; CAS 119340-53-3
beta-nicotinamide adenine dinuceotide (NAD +)	Millipore Sigma	Cat# N-1636; CAS 53-84-9
Rotenone	Millipore Sigma	Cat# 557368; CAS 83-79-4

REAGENT or RESOURCE	SOURCE	IDENTIFIER
Normal Goat Serum	Jackson ImmunnoResearch	Cat# 005-000-121; RRID:AB_2336990
Nicotinamide Riboside	Millipore Sigma	Cat# SMB00907; CAS 23111-00-4
Incucyte Cytotox Green Reagent	Essen Biosciences	Cat# 4633
PhosSTOP, phosphatase inhibitor cocktail	Millipore Sigma	Cat# 4906845001
Incucyte Cytolight Rapid Red Dye	Essen Bioscience	Cat# 4733
Fetal Bovine Serum, Heat Inactivated	ThermoFisher	Cat# 10500064
Critical Commercial Assays		
NF-Light ELISA	UMAN Diagnostics	Cat# 10-7001 CE
Radioligand binding selectivity panel	Eurofins Panlabs Discovery Services (Fremont, CA)	https://www.eurofinsdiscoveryservices.com
Biochemical selectivity assay	BPS Bioscience (San Diego, CA)	https://bpsbioscience.com/screening-and-profiling
Pierce BCA Protein Assay Kit	ThermoFisher	Cat# 23227
Experimental Models: Cell Lines		
NRK1-HEK293 Cells	Washington University, St. Louis	Essuman et al. (2017)
iPSC derived human motorneurons	Cellular Dynamics	iCell Motorneurons Cat# C1048
Experimental Models: Organisms/Strains		
Mouse: SARM1 B6.129X1-*Sarm1*^{tm1Aidi}/J	The Jackson Laboratory	IMSR Cat# JAX:018069 RRID: IMSR_JAX:018069
Mouse: wild type C57BL/6J	The Jackson Laboratory	RRID:IMSR_JAX:000664
Recombinant DNA		
PSF-CMV-AMP - CMV PROMOTER PLASMID	Millipore Sigma	Cat# OGS2
STREP-TEV-hSARM1$_{409-700}$	This paper	N/A
Software and Algorithms		
GraphPad Prism 8.4	GraphPad	https://www.graphpad.com/scientific-software/prism/
Columbus	PerkinElmer	https://www.perkinelmer.com/Product/image-data-storage-and-analysis-system-columbus
Other		
Jess Simple Western analyzer	ProteinSimple, San Jose, CA	Jess
Opera Phenix Scanner	PerkinElmer	Part# HH14000000
IncuCyte S3	Essen Bioscience, Ann Arbor, MI	N/A
SPE Cartridge	Spark, Holland	SPE 10 mm × 2 mm
Atlantis T3 Column	Waters, Milford, MA	Part# 186003719 (3 μm, 2.1 × 150 mm)
TSQ Quantiva Triple Quadrupole Mass Spectrometer	Thermo Scientific	N/A
Sorvall ST 16R Centrifuge	ThermoFisher	Cat# 75004380
Sonifier S450A	Branson Ultrasonics	Part# 101063198R
RapidFire 300 Mass Spectrometer	Agilent	N/A

REAGENT or RESOURCE	SOURCE	IDENTIFIER
API 4000 Triple Quad LC-MS/MS	SCIEX	N/A
IonMax/ESI Electrospray Ionization	Thermo Scientific	Cat# IQLAAEGABBFACTMAJI